American Mineralogist, Volume 96, pages 1199–1206, 2011

Brearleyite, $Ca_{12}Al_{14}O_{32}Cl_2$, a new alteration mineral from the NWA 1934 meteorite

Chi Ma,[1,*] Harold C. Connolly Jr.,[2,3,4] John R. Beckett,[1] Oliver Tschauner,[1,5] George R. Rossman,[1] Anthony R. Kampf,[6] Thomas J. Zega,[7] Stuart A. Sweeney Smith,[3,8] and Devin L. Schrader[4]

[1]Division of Geological and Planetary Sciences, California Institute of Technology, Pasadena, California 91125, U.S.A.
[2]Department of Physical Sciences, Kingsborough Community College of CUNY, Brooklyn, New York 11235, and Earth and Environmental Sciences, The Graduate Center of CUNY, New York, New York 10024, U.S.A.
[3]Department of Earth and Planetary Sciences, American Museum of Natural History, New York, New York 10024, U.S.A.
[4]Lunar and Planetary Laboratory, University of Arizona, Tucson, Arizona 85721, U.S.A.
[5]High Pressure Science and Engineering Center and Department of Geoscience, University of Nevada, Las Vegas, Nevada 89154, U.S.A.
[6]Mineral Sciences Department, Natural History Museum of Los Angeles County, Los Angeles, California 90007, U.S.A.
[7]Materials Science and Technology Division, Naval Research Laboratory, Washington, D.C. 20375, U.S.A.
[8]Department of Geology, Carleton College, Northfield, Minnesota 55057, U.S.A.

Abstract

Brearleyite (IMA 2010-062, $Ca_{12}Al_{14}O_{32}Cl_2$) is a Cl-bearing mayenite, occurring as fine-grained aggregates coexisting with hercynite, gehlenite, and perovskite in a rare krotite ($CaAl_2O_4$) dominant refractory inclusion from the Northwest Africa 1934 CV3 carbonaceous chondrite. The phase was characterized by SEM, TEM-SAED, micro-Raman, and EPMA. The mean chemical composition of the brearleyite is (wt%) Al_2O_3 48.48, CaO 45.73, Cl 5.12, FeO 0.80, Na_2O 0.12, TiO_2 0.03, –O 1.16, sum 99.12. The corresponding empirical formula calculated on the basis of 34 O+Cl atoms is $(Ca_{11.91}Na_{0.06})_{\Sigma 11.97}(Al_{13.89}Fe_{0.16}Ti_{0.01})_{\Sigma 14.06}O_{31.89}Cl_{2.11}$. The Raman spectrum of brealryeite indicates very close structural similarity to synthetic $Ca_{12}Al_{14}O_{32}Cl_2$. Rietveld refinement of an integrated TEM-SAED ring pattern from a FIB section quantifies this structural relationship and indicates that brearleyite is cubic, $I\bar{4}3d$; a = 11.98(8) Å, V = 1719.1(2) Å^3, and Z = 2. It has a framework structure in which AlO_4 tetrahedra share corners to form eight-membered rings. Within this framework, the Cl atom is located at a special position (3/8,0,1/4) with 0.4(2) occupancy and Ca appears to be disordered on two partially occupied sites similar to synthetic Cl-mayenite. Brearleyite has a light olive color under diffuse reflected light and a calculated density of 2.797 g/cm^3. Brearleyite is not only a new meteoritic Ca-,Al-phase, but also a new meteoritic Cl-rich phase. It likely formed by the reaction of krotite with Cl-bearing hot gases or fluids.

Keywords: Brearleyite, $Ca_{12}Al_{14}O_{32}Cl_2$, new mineral, Cl-bearing mayenite, NWA 1934 meteorite, CV3 carbonaceous chondrite, SAED ring pattern, Rietveld refinement

Introduction

A rare krotite ($CaAl_2O_4$)-dominant Ca-,Al-rich refractory inclusion (CAI), named "Cracked Egg" (Sweeney Smith et al. 2010), is observed in the Northwest Africa 1934 meteorite (a CV3 carbonaceous chondrite). Krotite is a newly discovered Ca-aluminate mineral (Ma et al. 2011). During our nanomineralogy investigation of this CAI, a Cl-bearing analog of mayenite, $Ca_{12}Al_{14}O_{32}Cl_2$, was also identified to be a new mineral, named "brearleyite." Electron probe microanalysis (EPMA), high-resolution scanning electron microscope (SEM), electron backscatter diffraction (EBSD), focused ion beam scanning electron microscope (FIB-SEM), transmission electron microscope (TEM), selected area electron diffraction (SAED), and micro-Raman analyses were used to characterize its composition and structure and those of associated phases. Synthetic $Ca_{12}Al_{14}O_{32}Cl_2$ is well known in the field of material science, showing a nanoporous cubic structure with a Ca-Al-O framework (Iwata et al. 2008). Pyrometamorphic phases structurally and chemically related to mayenites, $Ca_{13}Al_{14}(SiO_4)_{0.5}O_{32}Cl_2$ and $Ca_{13}Al_{14}(SiO_4)_4O_{24}Cl_4$, labeled as "chlormayenite" and "silicochlormayenite," respectively, were reported to occur in burnt dumps of the Chelyabinsk Coal Basin (Chesnokov 1999; Zateeva et al. 2007). Natural $Ca_{12}Al_{14}O_{32}Cl_2{\cdot}3H_2O$ was found in the Upper Chegem volcanic structure (Galuskin et al. 2009). We report here the first occurrence of $Ca_{12}Al_{14}O_{32}Cl_2$ in a meteorite, as an alteration mineral in a CAI. A preliminary description is given in Ma et al. (2010).

Mineral name and type material

The mineral and the mineral name (brearleyite) have been approved by the Commission on New Minerals, Nomenclature and Classification (CNMNC) of the International Mineralogical Association (IMA 2010-062). The name is for Adrian J. Brearley (1958-), a mineralogist at the University of New Mexico, in recognition of his many contributions to meteorite mineralogy. Three round thin sections (UA2169TS1, UA2169TS2, UA2169TS3) of one inch diameter contain the type material. Section UA2169TS1 is deposited under catalog USNM 7590 in the Smithsonian Institution's National Museum of Natural

* E-mail: chi@gps.caltech.edu

History, Washington, D.C. The three sections also contain type krotite (IMA 2010-038) (Ma et al. 2011).

Occurrence

The Northwest Africa (NWA) 1934 meteorite, found at an unrecorded location in northwest Africa, is a CV3 carbonaceous chondrite. The "Cracked Egg" CAI in the NWA 1934 meteorite is 2.75 mm × 4.50 mm in the section plane sampled by USNM 7590 and surrounded by a matrix of mostly fine-grained olivine. Krotite is the principal phase in the central and mantle regions in Cracked Egg (Ma et al. 2011). Brearleyite occurs with hercynite ($FeAl_2O_4$), gehlenite ($Ca_2Al_2SiO_7$), and perovskite ($CaTiO_3$) in veins and inclusions in the krotite ($CaAl_2O_4$) host and the entire assemblage is surrounded by a rim (Figs. 1–2). From inside toward the outside, the rim consists of grossite, mixed hibonite and spinel, then gehlenite ± spinel with an outer layer of Al-rich diopside. Gehlenite-rich or perovskite-rich domains also cut or occur in the rim but brearleyite was not identified in this region. Cracks, which crosscut the rim and portions of the interior, are mainly filled with Fe and Al hydrous oxides. Brearleyite in Cracked Egg is its first reported occurrence in a meteorite.

Appearance, physical and optical properties

The mineral occurs as small (80–300 nm) crystals forming fine-grained aggregates (1 × 1 μm to 20 × 60 μm in size) along with hercynite, gehlenite, and perovskite in veins and interstitial regions between krotite crystals within the krotite-dominant area of the CAI (Figs. 2–3).

In thin sections, brearleyite is optically transparent with a light olive color under a diffuse reflected light, based on Kelly and Judd's (1976) color scheme. Streak, luster, hardness, tenacity, cleavage, fracture, and density were not determined because of the small grain size. The density, calculated from the empirical formula is 2.797 g/cm^3. It is non-fluorescent under the electron beam of a scanning electron microscope. No crystal forms or twinning were observed.

Brearleyite is isotropic. The index of refraction could not be determined because the phase was only observed in thin section, but the Gladstone-Dale relationship predicts n = 1.600.

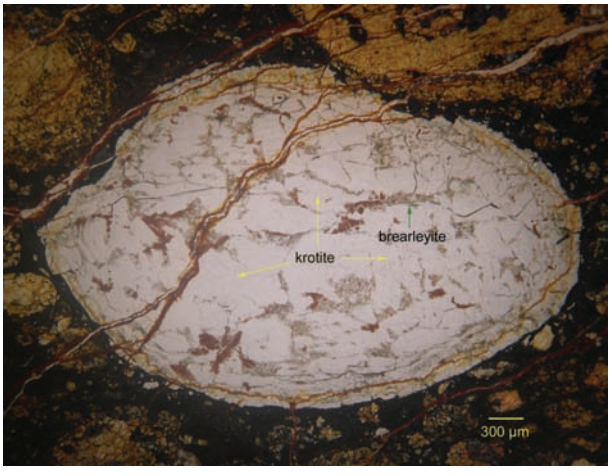

Figure 1. Photograph of the krotite-dominant CAI containing brearleyite, taken under a diffuse reflected light.

Raman spectroscopy

Raman microanalysis was carried out using a Renishaw M1000 micro-Raman spectrometer system and a 514.5 nm laser using methods described in Ma and Rossman (2008, 2009). The Raman spectrum of brearleyite (Fig. 4) is very close to that of

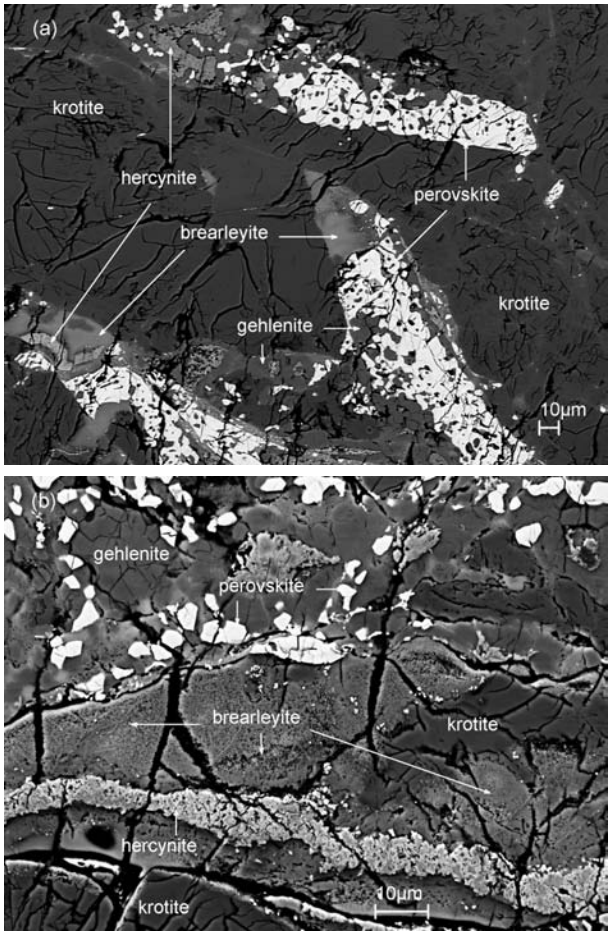

Figure 2. Backscattered electron images showing brearleyite with hercynite, perovskite, and gehlenite in the krotite host in two areas near the CAI center.

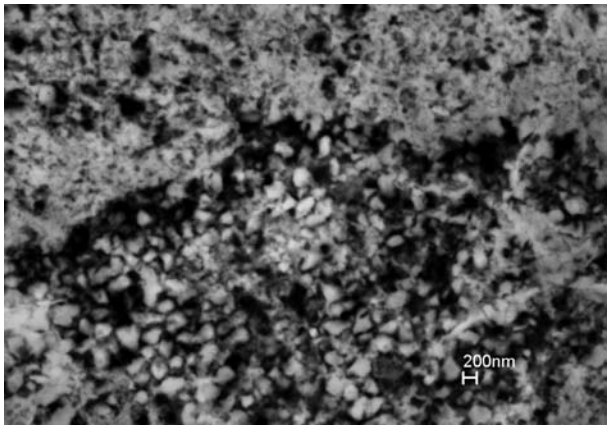

Figure 3. Backscattered electron image showing fine-grained brearleyite crystals.

synthetic $Ca_{12}Al_{14}O_{32}Cl_2$ (Sun et al. 2009), confirming that the meteoritic phase has a quite similar structure. The main spectral features are at 341 (E), 515 (A1, E, T2), 772 (T2), ~825, and ~879 cm^{-1}. The most intense bands are at 515 and 772 cm^{-1}. Mode assignments are derived from the calculated Raman spectrum of brearleyite based on force constants extracted from fitting the Raman spectrum of synthetic $Ca_{12}Al_{14}O_{32}Cl_2$ (Sun et al. 2009) using Vibratz (Dowty 2006). We note that in addition to the high mode degeneracy of the cubic symmetry the large unit cell with its 120 atoms implies strict overlaps of different eigenmodes at equal energies thus prohibiting unique assignments in absence of polarized Raman spectra from single-crystal specimens. Agreement between the observed and calculated modes is within a few cm^{-1} when using the refined structure model of brearleyite while the observed spectra of synthetic $Ca_{12}Al_{14}O_{32}Cl_2$ and brearleyite agree to within the spectral resolution of 1 cm^{-1}. In mayenite-like phases with other intrapore anions the observed energies of the Raman shifts are slightly different. For instance, in ozone-bearing $12CaO{\cdot}7Al_2O_3$ the most prominent peak is shifted from 515 to 520 cm^{-1} and the peak at 772 shifted to 780 cm^{-1} (Yang et al. 2004). Previous evaluations of Raman spectra of mayenite-type phases suggest that the mode at 515 and 520 cm^{-1}, respectively, is associated with the vibration of the lattice framework, while the shift at 780 cm^{-1} in ozone-bearing $12CaO{\cdot}7Al_2O_3$ has been attributed to vibrations involving O_2^{2-} (Yang et al. 2004). We note that the mass of Cl almost matches that of two O-atoms. Thus the equivalent vibrations in Cl-bearing $12CaO{\cdot}7Al_2O_3$ are expected to be in a very similar range of energy. We should mention that according to our calculations all modes at 515 and 772 cm^{-1} are associated with framework motion, whereas the peak at 341 cm^{-1} involves motion of Cl. However, our calculation did not include torsional and bending modes, which are a plausible origin of the Raman shifts at 825 and 879 cm^{-1}, but may also give rise to contributions of vibrations involving Cl to the multi-mode Raman peak at 772 cm^{-1}. Raman analysis gave no indication of either H_2O or OH^- in the 3200 to 3600 cm^{-1} region or of carbonate in the 1050 to 1100 cm^{-1} region. In addition to brearleyite features in the spectrum, there is a very broad, underlying band centered at about 2400 cm^{-1} from an unidentified laser-induced luminescence together with graphite bands superimposed in the 1400–1700 and 2500–3100 cm^{-1} regions originating from remnants of the carbon coat that was applied for the microbeam analyses and subsequently mostly removed.

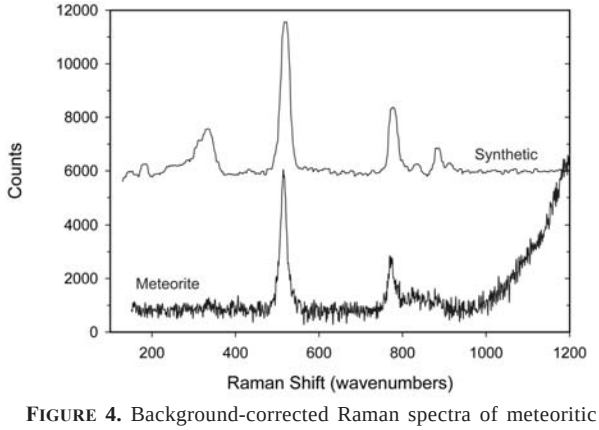

FIGURE 4. Background-corrected Raman spectra of meteoritic brearleyite (this study) and synthetic $Ca_{12}Al_{14}O_{32}Cl_2$ (Sun et al. 2009). The rise on the high-wavenumber end of the meteorite spectrum is from a graphite band arising from the remains of a carbon coat on the section used for analysis. Spectra have been displaced vertically for clarity.

CHEMICAL COMPOSITION

Chemical analyses of brearleyite and associated minerals were carried out using a JEOL 8200 electron microprobe (WDS mode, 15 kV, 25 nA, beam in focused mode). There was no Cl loss from brearleyite under the electron beam for the applied conditions. Standards for the analysis were spinel (Al*K*α, Mg*K*α), anorthite (Ca*K*α, Si*K*α), albite (Na*K*α), sodalite (Cl*K*α), synthetic fayalite (Fe*K*α), TiO_2 (Ti*K*α), and ZnO (Zn*L*α). Quantitative elemental microanalyses were processed with the CITZAF correction procedure and analytical results are given in Table 1. The empirical formula of brearleyite (based on O+Cl = 34) is $(Ca_{11.91}Na_{0.06})_{\Sigma 11.97}(Al_{13.89}Fe^{2+}_{0.16}Ti^{4+}_{0.01})_{\Sigma 14.06}O_{31.89}Cl_{2.11}$. Its ideal formula is $Ca_{12}Al_{14}O_{32}Cl_2$, which requires CaO 46.68, Al_2O_3 49.51, Cl 4.92, –O 1.11, total 100.00 wt%. The light olive color of type brearleyite may be due to a combination of Fe^{2+} and Fe^{2+}-Ti^{4+} charge transfer.

CRYSTALLOGRAPHY

FIB-TEM SAED ring pattern and Rietveld refinement

Because of the small grain size of brearleyite and its recognition only in thin section, X-ray powder diffraction data could not be obtained. Electron backscatter diffraction at a sub-micrometer scale was carried out on vibration-polished sections using the methods described in Ma and Rossman (2008, 2009) with an HKL EBSD system on a ZEISS 1550VP scanning electron microscope, operated at 20 kV and 6 nA in a focused beam with a 70° tilted stage. Brearleyite showed no EBSD pattern, due to small crystal sizes and/or deformation of surface layers by polishing, whereas associated minerals were identified by EBSD.

TABLE 1. The mean electron microprobe analytical results for brearleyite, hercynite, gehlenite, perovskite, and krotite

Constituent	Brearleyite n = 10	Hercynite n = 5	Gehlenite n = 3	Perovskite n = 3	Krotite n = 2
SiO_2	<0.04	0.06(5)	21.27(17)	0.58(9)	<0.04
TiO_2	0.03(1)	0.06(4)	0.28(5)	53.73(58)	<0.03
Al_2O_3	48.48(7)	63.75(67)	36.31(10)	1.64(13)	63.33(47)
FeO	0.80(3)	27.65(48)	0.21(3)	<0.04	<0.04
MgO	<0.02	0.02(2)	<0.02	<0.02	<0.02
CaO	45.73(13)	3.22(4)	41.71(23)	42.26(16)	36.24(12)
Na_2O	0.12(2)	0.25(6)	<0.02	<0.03	<0.02
Cl	5.12(3)	0.43(6)	<0.02	<0.02	<0.01
ZnO	<0.06	2.06(6)	<0.06	<0.08	<0.06
–O=Cl	–1.16				
Total	99.12	97.49	99.78	98.21	99.57
Based on O or O+Cl	34	4	7	3	4
Si		0.00	0.98	0.01	
Ti	0.01	0.00	0.01	0.93	
Al	13.89	2.13	1.97	0.04	1.98
Fe	0.16	0.66	0.01		
Mg		0.00			
Ca	11.91	0.10	2.06	1.04	1.03
Na	0.06	0.01			
Zn		0.04			
Cation sum	26.03	2.94	5.03	2.02	3.01

Notes: <*x*, where *x* stands for the detection limit at 99% confidence; (*y*) = one standard deviation; n = the number of analyses.

We prepared an electron-transparent cross section of brearleyite using an FEI Nova 600 (FIB-SEM) (Fig. 5a). The section was extracted with a micromanipulator and ion milled to electron transparency (100 to 150 nm) inside the FIB using previously described methods (Zega et al. 2007). Selected area electron diffraction patterns were acquired using a 200 keV JEOL 2200FS TEM. Based on the agreement between the Raman spectra of brearleyite and synthetic Cl-mayenite (Sun et al. 2009) and the very similar composition, the structures of both materials are expected to be very similar. Therefore, a refinement of the structure of synthetic Cl-mayenite using the integrated SAED ring pattern of brearleyite (Fig. 5b) is expected to converge to a set of meaningful structural parameters within the limits given by the quality of the diffraction data and may reveal eventual minor differences between the two materials. The Rietveld refinement was carried out with the program PowderCell (Kraus and Nolze 1996) after integration using Fit2D (Hammersley et al. 1996), as shown in Figure 6. Electron diffraction data for brearleyite are given in Table 2, structure refinement details are given in Table 3, and atom coordinates and displacement parameters in Table 4. The background functions in PowderCell are insufficient to model the background of the present pattern. Therefore we used a Tchebychev-polynomial fit in GSAS (Larson and Von Dreele 1994) with six fixed points to fit and subtract the background (GSAS does not accept primary beam energies as high as 200 keV, thus we could not use GSAS for structure refinement). For the same reason we had to subtract the background before Rietveld refinement in contrast to common praxis. However, the background is not highly structured and its subtraction should not affect the pattern fitting for Q below 4 A^{-1}. Diffraction peakprofiles were fitted best with purely Lorentzian functions using three profiles terms in PowderCell. Refinement of the structure was found stable with minimal shifts from the initial atom positions (Iwata et al. 2008) and all interatomic distances and angles are reasonable and in very good agreement with Boysen et al. (2007) (see Table 5). The wR_p was 0.23, R_p 0.16. PowderCell does not provide additional common figures of goodness of fit. We performed a Le Bail extraction (Le Bail et al. 1988; Kraus and Nolze 1996) with the Le Bail fit converging to an R_p of 0.09 and found a RF^2 of 0.25. In sum, the refinement factors, notably wR_p, are large. This opens the possibility of convergence of the Rietveld refinement to a local, unphysical, minimum. However, the very close similarity of the Raman spectra of brearleyite and synthetic $Ca_{12}Al_{14}O_{32}Cl_2$ supports the validity of the structure model to which the Rietveld refinement converged. We also checked for preferred orientation along the most misfit reflections 311 and 444 using the Rietveld-Toraya method but found that any potential preferred orientation is negligible. In sum, it is likely that the discrepancies between calculated and observed pattern are unsystematic and the result of insufficient powder statistics. In fact, the diffraction pattern in Figure 5b shows that the Debye fringes are spotty and excellent refinement parameters are not to be expected.

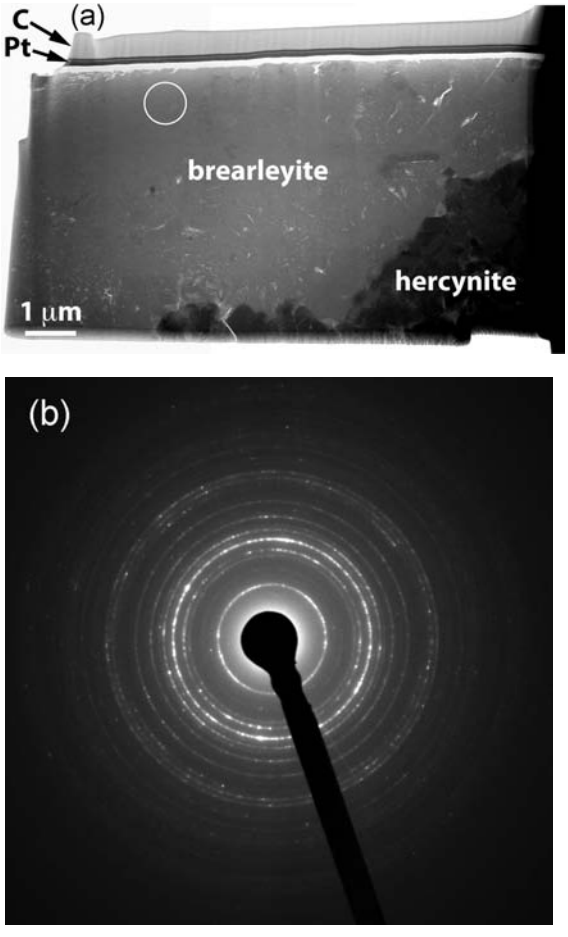

FIGURE 5. TEM data on brearleyite. (**a**) Bright-field scanning TEM mosaic of a FIB section of brearleyite and hercynite. Protective layers of Pt and C were deposited on top of the brearleyite prior to sectioning to mitigate radiation damage and Ga^+ ion implantation. (**b**) Selected area electron diffraction pattern of brearleyite nano-crystals acquired from the region of the FIB section enclosed by the white circle in **a**.

Mayenite-type materials are known to exhibit disorder of the calcium ions. Therefore, we examined the observed electron powder diffraction pattern of brearleyite for indications of such disorder. We examined convergence of the refinement with (1) Ca distributed on two Wyckoff sites 24*d* (Bartl and Scheller 1970) and varying the occupancy of both sites between 0 and 1; and (2) varying the Ca occupancy on these two sites as before and additionally varying the Cl-occupancy between 0 and 1. The latter procedure was chosen because the anion partial occupancy of the cages in the mayenite-lattice correlates with cation disorder (Boysen et al. 2007). We found that both procedures, particularly the latter, improve the refinement. Furthermore, we found that the partial occupancies of the two Ca-sites add up to ~1 even without constraining the sum. The noticeable statistical deviations between observed and calculated intensities limit the reliability of refining subtle structural effects such as cation-site disorder. However, within the error margins (Table 4), the Rietveld refinement supports the presence of this disorder. Interatomic distances, including those between Ca and O, are similar to those reported by Boysen et al. (2007) who explicitly modeled Ca- and interstitial anion disorder. We present the interatomic distances of the refined structure model for brearleyite in Table 5. The Rietveld refined structure yields a space group and unit-cell parameters of $I\bar{4}3d$; a = 11.979(77)

TABLE 2. Electron diffraction data for brearleyite

d_{obs}	I_{obs}	I_{calc}	h k l
4.898(12)	17.2	14.8	2 1 1
4.242(10)	1.2	0.1	2 2 0
3.795(9)	2.1	4.4	3 1 0
3.208(7)	14.2	18.6	3 2 1
3.001(7)	**47.1**	38.1	4 0 0
2.685(6)	**100**	100	4 2 0
2.559(6)	14.4	11.1	3 3 2
2.451(5)	**54.9**	59.5	4 2 2
2.355(5)	0.2	0.1	4 3 1
2.355(5)	13.6	13.4	5 1 0
2.192(5)	**32.7**	38	5 2 1
2.123(4)	0.3	0	4 4 0
2.059(4)	6.5	7.1	5 3 0
1.947(4)	**24.1**	33.3	5 3 2
1.947(4)	0.7	0.7	6 1 1
1.899(4)	2.6	5.2	6 2 0
1.852(4)	4.9	3.6	5 4 1
1.770(3)	7	8.5	6 3 1
1.733(4)	8.7	20.8	4 4 4
1.698(4)	2.4	3.7	5 4 3
1.698(4)	9	5.5	7 1 0
1.665(4)	**42**	89.2	6 4 0
1.634(4)	3	7.3	6 3 3
1.634(4)	0.4	1.2	7 2 1
1.634(4)	8.3	9.3	5 5 2
1.604(3)	**60.8**	78.1	6 4 2
1.576(4)	0.7	0.8	7 3 0
1.525(3)	6.1	14.2	7 3 2
1.525(3)	7.5	18.1	6 5 1
1.501(3)	11.1	20	8 0 0
1.478(3)	15.7	13.6	7 4 1
1.456(3)	2.4	2.8	8 2 0
1.435(3)	8.4	7.1	6 5 3
1.415(3)	2	2.3	8 2 2
1.415(3)	1.3	4.1	6 6 0
1.396(3)	16.7	22.1	7 4 3
1.396(3)	1.7	4.2	8 3 1
1.396(3)	12.3	18.7	7 5 0
1.359(3)	11.6	7.4	7 5 2
1.342(3)	13.9	22.9	8 4 0
1.310(11)	3.9	0.7	9 1 0
1.310(3)	**22.3**	44.5	8 4 2
1.295(3)	1.5	2.6	9 2 1
1.295(3)	1.5	1.3	7 6 1
1.295(3)	5	6.3	6 5 5
1.266(10)	12.6	14.7	6 6 4
1.266(3)	3.4	0.7	9 3 0
1.266(3)	8.9	6.4	7 5 4
1.266(3)	5.9	6.4	8 5 1
1.238(3)	9.5	4.5	9 3 2
1.238(3)	1.2	2.4	7 6 3
1.225(3)	3.7	4	8 4 4
1.213(2)	9.5	4.3	8 5 3
1.213(2)	10.8	1.6	9 4 1
1.201(2)	3.2	3.5	8 6 0
1.189(2)	3.3	0.5	10 1 1
1.189(2)	2.2	1.6	7 7 2
1.177(2)	16.8	21.8	10 2 0
1.177(2)	0.5	1.4	8 6 2
1.166(2)	2.5	1.3	9 4 3
1.166(2)	1.3	0	9 5 0
1.145(2)	5	9.2	9 5 2
1.145(2)	5.7	5.9	10 3 1
1.145(2)	5.6	2.1	7 6 5
1.125(2)	4.7	5.2	8 7 1
1.115(2)	11.2	27.8	8 6 4
1.115(2)	15.1	31.7	10 4 0
1.106(2)	0.9	4.4	9 6 1
1.106(2)	5.6	13.5	10 3 3
1.096(2)	17.6	20.6	10 4 2
1.087(2)	6.7	2.4	9 5 4
1.087(2)	0	0.2	11 1 0
1.087(2)	10.6	15.6	8 7 3
1.070(2)	3.2	5	9 6 3
1.070(2)	4.5	4.3	10 5 1
1.070(2)	9.4	4.1	11 2 1
1.061(2)	15	36.8	8 8 0
1.053(2)	1.2	2.3	11 3 0
1.053(2)	6.8	3.6	9 7 0
1.038(2)	13.9	16.7	11 3 2
1.038(2)	3.5	1.6	10 5 3
1.038(2)	0.3	0.6	7 7 6
1.038(2)	2.2	2.2	9 7 2
1.030(2)	1.2	0.9	8 6 6
1.030(2)	3.3	3.7	10 6 0
1.022(2)	2.6	0.3	8 7 5
1.022(2)	2.3	1.1	11 4 1
1.015(2)	2.2	0.4	10 6 2
1.007(2)	6.7	4.2	9 6 5
1.001(2)	0.4	1.6	8 8 4
1.001(2)	3.4	2.8	12 0 0
0.994(2)	4.8	1.5	9 7 4
0.994(2)	0.1	0.2	9 8 1
0.994(2)	3.9	5.5	11 4 3
0.994(2)	0	0.6	11 5 0
0.987(2)	8.9	33.1	12 2 0
0.980(2)	1.4	1	10 7 1
0.980(2)	0.3	0.1	11 5 2
0.980(2)	1.4	0.5	10 5 5
0.974(2)	9.3	14	10 6 4
0.974(2)	3.2	7.7	12 2 2
0.968(2)	2.7	1.3	12 3 1
0.968(2)	1.8	3.3	9 8 3
0.956(2)	12.8	2.9	10 7 3
0.956(2)	2.9	0.9	11 6 1

Note: The 8 strongest lines are in bold.

Å, V = 1719.12(22) Å^3, and Z = 2; CIF data[1] for brearleyite is on deposit.

Crystal structure

The refined structure shows 0.4(2) occupancy of Cl and a slightly different distribution of Ca on the two competing sites than reported by Iwata et al. (2008). A drawing of the structure is provided in Figure 7. Like other phases assuming the mayenite-type structure, brearleyite has a framework structure in which AlO_4 (aluminate) tetrahedra share corners to form eight-membered rings. The aluminate framework of mayenites establishes a rigid nano-porous framework with Ca and additional anions necessary for charge balance (O, Cl, …) residing within the pores of this framework (Boysen et al. 2007 and references within). Both Ca and these additional not-framework bound anions are commonly heavily disordered (Bartl and Scheller 1970; Boysen et al. 2007). In brearleyite within this framework, the Cl atom is located at a special position (3/8,0,1/4) and Ca is disordered on two partially occupied sites (Bartl and Scheller 1970; Boysen et al. 2007). The Cl site corresponds to the O3 site described in earlier reports of the structure of mayenite (e.g., Boysen et al. 2007) as being surrounded by a "cage" formed by the aluminate framework and Ca sites.

ASSOCIATED HERCYNITE

Hercynite is in close association with brearleyite (Figs. 2 and 5a), occurring as fine-grained aggregates. It contains significant amounts of Ca and Zn (Table 1), showing a formula of

[1] Deposit item AM-11-041, CIF. Deposit items are available two ways: For a paper copy contact the Business Office of the Mineralogical Society of America (see inside front cover of recent issue) for price information. For an electronic copy visit the MSA web site at http://www.minsocam.org, go to the *American Mineralogist* Contents, find the table of contents for the specific volume/issue wanted, and then click on the deposit link there.

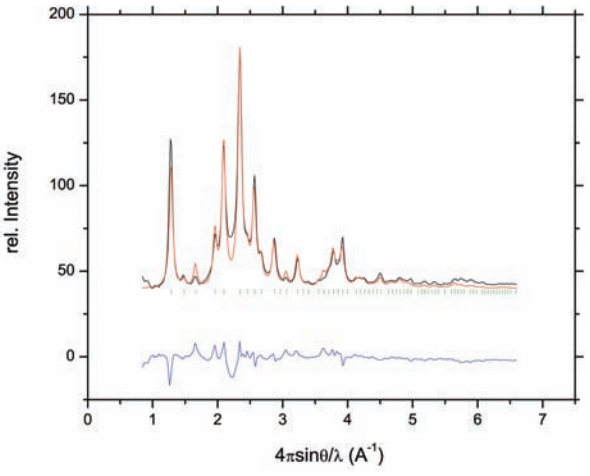

FIGURE 6. Rietveld refinement of the integrated SAED pattern with PowderCell with integration using Fit2D. Black = experimental, red = calculated, blue = residual, tick marks = reflection angles; wR_p = 0.23. The wR_p is not very good and we attribute this to the spottiness of the SAED ring pattern because the structure remained stable upon refinement with minimal shifts from the initial atom positions (Iwata et al. 2008) and because all interatomic distances and angles are reasonable. We also checked for preferred orientation using the Rietveld-Toraya method but found that any potential preferred orientation is negligible.

TABLE 3. Structure refinement details for brearleyite

Cell full formula	$Ca_{26.722}Al_{27.998}O_{63.998}Cl_{4.488}$
Formula atomic weight	3009.43
Crystal system	cubic
Space group	$I\bar{4}3d$
Unit-cell dimension	a = 11.98(8) Å
Cell volume	1719.1(2) Å^3
Density, calculated	2.907 g/cm^3
Pearson code	cI152
Formula type	N3O7P12Q16
Wyckoff sequence	ed^{2}c^{2}ba

TABLE 4. Atom coordinates and isotropic displacement parameters (Å^2)

Atom	Wyck.	Occ.	*x/a*	*y/b*	*z/c*
Ca1	24*d*	0.77(11)	0.615(5)	0	1/4
Ca2	24*d*	0.34(11)	0.555(7)	0	1/4
Al1	16*c*	1	0.013(3)	0.013(3)	0.013(3)
Al2	12*b*	1	7/8	0	1/4
O1	48*e*	1	0.792(2)	0.095(5)	0.30(1)
O2	16*c*	1	0.170(34)	0.170(34)	0.170(34)
Cl	12*a*	0.37(17)	3/8	0	1/4

$(Fe^{2+}_{0.66}Al_{0.13}Ca_{0.10}Zn_{0.04})_{\Sigma 0.93}Al_2O_4$. Its EBSD patterns are weak but reveal a spinel structure. Some grains have a high alumina core, which may indicate corundum. Hercynite is an alteration phase in Cracked Egg, similar to that identified in altered CAIs from the Allende (CV3; Ma 2010) and Lancé (CO3; Fahey et al. 1998) chondrites.

DISCUSSION

Brearleyite ($Ca_{12}Al_{14}O_{32}Cl_2$) is the Cl analog of mayenite ($Ca_{12}Al_{14}O_{33}$) with space group $I\bar{4}3d$. It is not only a new meteoritic Ca-,Al-phase, but also a new Cl-rich phase, joining the Cl-rich meteoritic minerals sodalite ($Na_4Al_3Si_3O_{12}Cl$) and wadalite ($Ca_6Al_5Si_2O_{16}Cl_3$).

TABLE 5. Selected bond lengths (Å) and angles (°)

Atom1	Atom2	Distance	
Ca1	Al2	3.11(8)	
Ca1	O1	2.52(2)	
Ca1	Cl	2.88(4)	
Ca1	O1	2.28(19)	
Ca1	O2	2.44(10)	
Ca2	O1	3.15(8)	
Ca2	Cl	2.15(8)	
Ca2	O1	2.31(22)	
Ca2	O2	2.37(7)	
Al2	O1	1.70(6)	
O1	Al1	1.87(3)	
O2	Al1	1.70(17)	
Atom1	Atom2	Atom3	Angle
Ca2	Ca1	O1	85.6(1.4)
Ca1	Ca2	O2	87.7(4.9)
O1	Ca1	Cl	149.4(6)
O1	Ca1	O1	71.0(8)
O1	Al2	O1	111.97(23)
Al2	O1	Ca1	122(3)
Al2	O1	Ca2	108(3)
Al2	O1	Al1	142 (3)
O1	Ca1	O2	92(3)
O1	Ca1	O1	171(3)
O1	Al1	O1	105 (4)
Ca1	Cl	Ca2	0.0(1)

* The data compare well to the results of Boysen et al. (2007) who used neutron powder diffraction and considered Ca and O- disorder and partial occupancies explicitly.

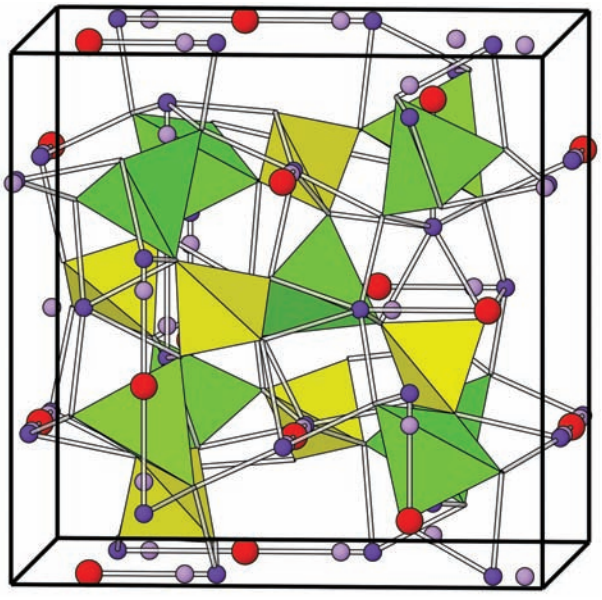

FIGURE 7. Crystal structure of brearleyite. $Al1O_4$ and $Al2O_4$ tetrahedra are green and yellow, respectively. Ca1 and Ca2 atoms are dark purple and light purple, respectively. Bonds to the Ca2 site are omitted for clarity. Cl atoms are red. The solid black lines outline one unit cell.

Late-stage alteration is often observed in CV3 chondrites; it occurred in nebular environments as well as on the parent body and led to the introduction of various amounts of Na, Cl, and oxidized Fe into CAIs (Krot et al. 1995; Brearley 2005). Brearleyite is apparently an alteration phase in Cracked Egg, likely formed by iron-alkali-halogen metasomatism along with hercynite, replacing primary phase(s) in the CAI.

The specific reactions that took place during alteration and the

phases that were most affected depend strongly on the primary phase assemblage. We, therefore, begin with a brief overview of the pre-alteration history of Cracked Egg and then consider the interaction of this primary phase assemblage with an altering medium. Currently, the Cracked Egg CAI consists mostly of large krotite crystals with interstitial phase assemblages consisting of gehlenite, perovskite, hercynite, and brearleyite. There are also a few hexamolybdenum crystals included in krotite near the outer margins of the inclusion. Surrounding the entire inclusion is a rim sequence consisting from inside toward the outside of grossite → hibonite + spinel → gehlenite ± spinel → aluminous diopside. The grossite also contains inclusions of hexamolybdenum. The outer pyroxene appears to be later than the rest of the rim and, therefore, unrelated to the rim formation event, so we ignore it for present purposes, but the other phases are consistent with a layer sequence formed by the reaction of krotite with a gas and we consider it first because it is an important time marker. We can constrain the nature of this vapor by writing reactions at each interface between the successive rims and between krotite, the principal substrate, and overlying grossite. At equilibrium, we have for example

$$CaAl_2O_4 + 2Al\ (gas) + 1.5O_2\ (gas) = CaAl_4O_7\ (grossite)$$

which states that the gas must be contributing Al. To avoid specifying an oxygen fugacity, we recast this as

$$CaAl_2O_4 + Al_2O_3\ (corundum) = CaAl_4O_7\ (grossite).$$

Using the FactSage 6.1 database, we obtain log aAl_2O_3 of –0.6 referenced to 1000 °C. Similar reactions can be written for the grossite – spinel + hibonite and spinel + hibonite – melilite ± spinel interfaces, leading to log aAl_2O_3 values of –0.6, –0.06, and –0.03, respectively, from inside toward the outside (i.e., the gas, if at 1000 °C, would have been very nearly corundum saturated). Since we do not observe corundum in the rim, this suggests that the rim-forming process probably occurred at temperatures above 864 °C because corundum would have been stabilized in the rim at lower temperatures and would, therefore, have been observed in the rim sequence unless kinetically inhibited from forming. A similar analysis for CaO, leads to the conclusion that the gas was lower in Ca than needed to stabilize krotite. Overall, the rim-forming event took place at elevated temperatures (>864 °C) in a refractory gas (high chemical potential for Al_2O_3).

Prior to the rim-forming event, Cracked Egg would have been a krotite-dominant phase assemblage but additional, mostly interstitial, phases were also present. Hexamolybdenum is observed as inclusions in krotite near the rim (also in grossite derived from near-rim krotite) and, therefore, it formed before these crystals but it is not found in other phases and, in particular, it is not found in the interior krotite crystals or in the interstitial regions between them. This suggests that the bulk of the krotite (those crystals in the interior of the inclusion) formed before (or in a different place) than the hexamolybdenum, which is found only in the outermost portions of the inclusion. Perovskite and gehlenite are known to be stable at high temperature for a broad range of vapor compositions (e.g., Ebel 2006) but hercynite and, presumably, brearleyite were not. One simple possibility is that krotite reacted with a Cl-bearing vapor to form brearleyite and corundum, the overall reaction being

$$12CaAl_2O_4\ (krotite) + Cl_2\ (gas) \rightarrow Ca_{12}Al_{14}O_{32}Cl_2\ (brearleyite) + 5Al_2O_3\ (corundum) + 0.5O_2,$$

with later conversion of corundum to hercynite through interaction with an Fe-bearing fluid via

$$Al_2O_3\ (corundum) + FeO\ (gas) = FeAl_2O_4\ (hercynite).$$

We posit a sequential formation of brearleyite and hercynite because of the highly aluminous cores of some hercynite crystals, which would imply initial formation of corundum rather than hercynite. It may be, however, that although corundum and brearleyite were the initial products of krotite–vapor interactions, hercynite, and brearleyite were the products later in the same event (i.e., corundum did not react with a gas to form hercynite but hercynite supplanted corundum as a reaction product of krotite as the metasomatic event proceeded). Zinc in the hercynite was probably introduced at the same time as the Fe. Note that our use of "FeO" in the above hercynite formation reaction is not intended to imply that the dominant vapor species for Fe was FeO. Other Fe-bearing species [e.g., Fe, $Fe(OH)_2$, etc.] may have been more important but the selected equation is a convenient description of phase changes among the solids. Mobility of Fe during parent body or nebular metasomatism of CAIs in CV3 chondrites is well known (e.g., Brearley and Jones 1998) and peak temperatures for the metasomatic event that introduced Fe into $MgAl_2O_4$-rich spinels from CAIs in the Allende CV3 meteorite are constrained to ~600–700 °C (Paque et al. 2007). Conversion of corundum to hercynite also likely requires relatively high temperatures for kinetic reasons (e.g., the reaction would be quite slow for temperatures below ~400 °C); required temperatures for brearleyite formation and krotite reaction with Cl-,Fe-bearing fluids are unknown.

An alternative possibility to the alteration of krotite to produce brearleyite, as presented above, is that the precursors to hercynite and brearleyite were corundum, as suggested above, and mayenite and that both phases were part of the pre rim-forming inclusion. In this type of model, mayenite and corundum were later altered to brearleyite and hercynite during a metasomatic event. We see no evidence for internal decomposition of the krotite, so pure krotite was stable relative to mayenite plus corundum and, therefore, formation of mayenite/corundum would have occurred through surface controlled reactions involving krotite. This class of scenarios can be envisioned in terms of either a melting or a metasomatic event. If mayenite formed during a melting event, some fraction of the presumably original perovskite, gehlenite, and krotite dissolved into the melt. The silicate and perovskite components in the melt eventually recrystallized as gehlenite and perovskite but some fraction of the krotite-derived oxides crystallized to form mayenite and corundum, i.e., the process was potentially isochemical so that $12CaAl_2O_4\ (krotite) \rightarrow Ca_{12}Al_{14}O_{33}\ (mayenite) + 5Al_2O_3$ (corundum), which predicts a molar mayenite/corundum ratio of 1/5. If mayenite and corundum crystallized from a melt, they likely formed within chemical potential gradients caused by zoning within the melt or crystallized at different times, as these two phases generally occupy distinct regions of the veins/interstices

between krotite grains (e.g., Fig. 2). Temperatures for this putative melting event are poorly constrained because perovskite-saturated liquid compositions in such Al-rich silicate melts have not been studied experimentally but they are likely to be above the >1350 °C needed for krotite-saturated melts in the CaO-Al_2O_3-SiO_2 system and below those of the gehlenite-spinel eutectic (1527 °C). Upon crystallization, the inclusion would have appeared very similar to the observed inclusion except that mayenite and corundum would have been present but not brearleyite or hercynite. The formation of these latter two phases would reflect a later alteration event. Mayenite produced by crystallization may have reacted with a hot Cl-,Fe-rich vapor to produce brearleyite as in

$$Ca_{12}Al_{14}O_{33}\ (\text{mayenite}) + Cl_2\ (\text{gas}) = Ca_{12}Al_{14}O_{32}Cl_2\ (\text{brearleyite}) + 0.5O_2.$$

We view scenarios with the intermediate presence of mayenite to be inherently less likely than the simple metasomatic reactions discussed above. Aside from having to appeal to unknown phase relations, the primary difficulties with models involving precursor mayenite are the required destruction of all mayenite to form brearleyite and postulating the previous existence of a now absent phase, mayenite, for which there is no direct evidence. We view a metasomatic reaction of krotite to form brearleyite and corundum/hercynite as more likely.

Finally, we note that we cannot completely exclude the possibility that brearleyite is a terrestrial alteration product after mayenite. NWA 1934 is a weathered find (W3) and, during its time on the Earth, weathering has destroyed most of the metal and sulfides originally present in the meteorite. If brearleyite is terrestrial, then complete conversion of mayenite, if it was present, to brearleyite is a requirement or, one must postulate that dissolution-precipitation reactions involving krotite in aqueous solutions would yield the observed brearleyite plus hercynite.

We observed no mayenite in "Cracked Egg" despite careful searches and, as noted above, a hercynite/corundum reaction probably requires higher temperatures than would be available during weathering. Also, a robust source of Cl is required. Chlorine enhancements in Antarctic meteorites are well known and reflect contributions from sea salts, but hot desert finds usually do not display major bulk enhancements in Cl although they are observed (e.g., Lee and Bland 2004) and, since the sample locality is unknown, a near-shore or playa environment cannot be excluded. Overall, we view a terrestrial origin for brearleyite as possible but contrived and that a preterrestrial origin for brearleyite is much more likely.

ACKNOWLEDGMENTS

SEM, EBSD, and EPMA analyses were carried out at the Caltech GPS Division Analytical Facility, which is supported, in part, by grant NSF EAR-0318518 and the MRSEC Program of the NSF under DMR-0080065. FIB and TEM work was performed at the Naval Research Laboratory. This research was also supported by NSF REU grant AST 0851362 and NASA OSS Grant NNX09AB86G (to H.C.C. Jr.), NNX09AG40G (to E.M. Stolper), and NNH09AK541 (to T.J.Z.), and NSF grant EAR-0337816 (to G.R.R.), and NNSA Cooperative Agreement DE-FC88-01NV14049 (to O.T.). We thank F. Colombo, C.M. Gramaccioli, and J.C. Melgarejo for constructive reviews of this manuscript.

REFERENCES CITED

Bartl, H. and Scheller, T. (1970) Zur Struktur des $12CaO{\cdot}7Al_2O_3$. Neues Jahrbuch für Mineralogie Monatshefte, 547–552.

Boysen, H., Lerch, M., Stys, A., and Senyshyn, A. (2007) Structure and oxygen mobility in mayenite ($Ca_{12}Al_{14}O_{33}$): A high-temperature neutron powder diffraction study. Acta Crystallographica B, 63, 675–682.

Brearley, A.J. (2005) Nebular versus parent-body processing. In A.M. Davis, Ed., Meteorites, Comets, and Planets, 1, p. 247–268. Treatise on Geochemistry, Elsevier, Amsterdam.

Brearley, A.J. and Jones, R.H. (1999) Chondritic meteorites. In J.J. Papike, Ed., Planetary Materials, 36, p. 3-1–3-398. Reviews in Mineralogy, Mineralogical Society of America, Chantilly, Virginia.

Chesnokov, B.V. (1999) Experience in technogenic mineralogy: 15 years on burnt dumps of underground and opencast coal mines and concentrating plants of the Southern Urals. Ural'skii Mineralogicheskii Sbornik, 9, 138–167.

Dowty, E. (2006) VIBRATZ. Shape Software, Kingsport, Tennessee, U.S.A.

Ebel, D.S. (2006) Condensation of rocky material in astrophysical environments. In D.S. Lauretta and H.Y. McSween Jr., Eds., Meteorites and the Early Solar System II, pp. 253–277. University of Arizona Press, Tucson.

Fahey, A.J., Zinner, E., Kurat, G., and Kracher, A. (1998) Hibonite-hercynite inclusion HH-1 from the Lancé (CO3) meteorite: The history of an ultrarefractory CAI. Geochimica et Cosmochimica Acta, 58, 4779–4793.

Galuskin, E.V., Gazeev, V.M., Lazic, B., Armbruster, T., Galuskina, I.O., Zadov, A.E., Pertsev, N.N., Wrzalik, R., Dzierżanowski, P., Gurbanov, A.G., and Bzowska, G. (2009) Chegemite $Ca_7(SiO_4)_3(OH)_2$—A new humite-group calcium mineral from the Northern Caucasus, Kabardino-Balkaria, Russia. European Journal of Mineralogy, 21, 1045–1059.

Hammersley, A.P., Svensson, S.O., Hanfland, M., Fitch, A.N., and Hausermann, D. (1996) Two-dimensional detector software: From real detector to idealised image or two-theta scan. High Pressure Research, 14, 235–248.

Iwata, T., Haniuda, M., and Fukuda, K. (2008) Crystal structure of $Ca_{12}Al_{14}O_{32}Cl_2$ and luminescence properties of $Ca_{12}Al_{14}O_{32}Cl_2$:Eu^{2+}. Journal of Solid State Chemistry, 181, 51–55.

Kelly, K.L. and Judd, D.B. (1976) Color: Universal Language and Dictionary of Names. National Bureau of Standards Special Publication, 440, 158 pp.

Kraus, W., and Nolze, G. (1996) POWDER CELL—a program for the representation and manipulation of crystal structures and calculation of the resulting X-ray powder patterns. Journal of Applied Crystallography, 29, 301–303.

Krot, A.N., Scott, E.R.D., and Zolensky, M.E. (1995) Mineralogical and chemical modification of components in CV3 chondrites: Nebular or asteroidal processing? Meteoritics, 30, 748–775.

Larson, A.C. and Von Dreele, R.B. (1994) General Structure Analysis System (GSAS), Los Alamos National Laboratory Report LAUR 86-748.

Le Bail, A., Duroy, H., and Fourquet, J.L. (1988) Ab-initio structure determination of $LiSbWO_6$ by X-ray powder diffraction. Materials Research Bulletin, 23, 447–452.

Lee, M.R. and Bland, P.A. (2004) Mechanisms of weathering of meteorites recovered from hot and cold deserts and the formation of phyllosilicates. Geochimica et Cosmochimica Acta, 68, 893–916.

Ma, C. (2010) Hibonite-(Fe), $(Fe,Mg)Al_{12}O_{19}$, a new alteration mineral from the Allende meteorite. American Mineralogist, 95, 188–191.

Ma, C. and Rossman, G.R. (2008) Barioperovskite, $BaTiO_3$, a new mineral from the Benitoite Mine, California. American Mineralogist, 93, 154–157.

——— (2009) Tistarite, Ti_2O_3, a new refractory mineral from the Allende meteorite. American Mineralogist, 94, 841–844.

Ma, C., Sweeney Smith, S.A., Connolly Jr., H.C., Beckett, J.R., Rossman, G.R., and Schrader, D.L. (2010) Discovery of Cl-bearing mayenite, $Ca_{12}Al_{14}O_{32}Cl_2$, a new mineral in a CV3 meteorite. Meteoritics and Planetary Science, 45, Supplement, A123.

Ma, C., Kampf, A.R., Connolly Jr., H.C., Beckett, J.R., Rossman, G.R., Sweeney Smith, S.A., and Schrader, D.L. (2011) Krotite, $CaAl_2O_4$, a new refractory mineral from the NWA 1934 meteorite. American Mineralogist, 95, 709–715.

Paque, J.M., Burnett, D.S., and Beckett, J.R. (2007) Zoning patterns of Fe and V in spinel from a type B Ca-Al-rich inclusion: Constraints on subsolidus thermal history. Meteoritics and Planetary Science, 42, 899–912.

Sun, J.Q., Song, C.F., Ning, S., Lin, S.B., and Li, Q.X. (2009) Preparation and characterization of storage and emission functional material of chlorine anion: $[Ca_{24}Al_{28}O_{64}]^{4+}{\cdot}(Cl^-)_{(3.80)}(O^{2-})_{(0.10)}$. Chinese Journal of Chemical Physics, 22, 417–422.

Sweeney Smith, S.A., Connolly Jr., H.C., Ma, C., Rossman, G.R., Beckett, J.R., Ebel, D.S., and Schrader, D.L. (2010) Initial analysis of a refractory inclusion rich in $CaAl_2O_4$ from NWA 1934: Cracked Egg. 41st Lunar and Planetary Science Conference, Abstract 1877.

Yang, S., Kondo, J.N., Hayashi, K., Hirano, M., Domen, K., and Hosono, H. (2004) Formation and desorption of oxygen species in nanoporous crystal $12CaO{\cdot}7Al_2O_3$. Chemistry of Materials, 16, 104–110.

Zateeva, S.N., Sokol, E.V., and Sharygin, V.V. (2007) Specificity of pyrometamorphic minerals of the ellestadite group. Geology of Ore Deposits, 49, 792–805.

Zega, T.J., Nittler, L.R., Busemann, H., Hoppe, P., and Stroud, R.M. (2007) Coordinated isotopic and mineralogic analyses of planetary materials enabled by in situ lift-out with a focused ion beam scanning electron microscope. Meteoritics and Planetary Science, 42 1373–1386.

MANUSCRIPT RECEIVED DECEMBER 5, 2010
MANUSCRIPT ACCEPTED APRIL 13, 2011
MANUSCRIPT HANDLED BY FERNANDO COLOMBO